Supporting Information for

Gas-Phase Formation of Silicon Dicarbide (c-SiC_2): A Key Cyclic Precursor to Silicon Carbide Grains in Space

Shane J. Goettl,[a] Iakov A. Medvedkov,[a] Zhenghai Yang,[a] Surajit Metya,[a] Márcio O. Alves,[b] Breno R. L. Galvão,[b]* Ralf I. Kaiser[a]*

[a] Department of Chemistry, University of Hawai'i at Mānoa, Honolulu, HI 96822, USA

[b] Centro Federal de Educação Tecnológica de Minas Gerais, 30421-169, Belo Horizonte, MG, Brazil

Correspondence: ralfk@hawaii.edu, brenogalvao@gmail.com

Materials and Methods

The bimolecular reaction of dicarbon (C_2, $X^1\Sigma_g^+$ / $a^3\Pi_u$) with the silylidyne radical (SiH, $X^2\Pi$) was conducted under single collision conditions utilizing the crossed molecular beam technique.[1-7] A pulsed supersonic dicarbon beam was generated *in situ* via laser ablation of a rotating graphite rod using the 266 nm output of a Nd:YAG laser (Quanta-Ray Pro 270, Spectra-Physics) at 30 Hz and 3–6 mJ per pulse. The ablated species were seeded in helium (He, 99.9999 %, Matheson) at a backing pressure of 3,000 Torr pulsed at 60 Hz, −400 V amplitude, and a pulse width of 80 μs. The reactant beam passed through a skimmer and was velocity-selected by a chopper wheel giving a peak velocity (v_p) and speed ratio (S) of 1912 ± 62 m s^{-1} and 3.9 ± 0.4, respectively. A pulsed beam of dilute disilane (99.998%, Air Liquide) at a fraction of 0.5 % in helium and a backing pressure of 1150 Torr was fed into a piezoelectric valve operating with the same parameters as for the dicarbon beam, which was intercepted by a 1 mm × 4 mm laser spot from a 193 nm ArF excimer laser (COMPex 110, Coherent, 30 Hz, 15 mJ per pulse) located 1 mm downstream from the nozzle. The resulting silylidyne beam (v_p = 1698 ± 8 m s^{-1}, S = 16.3 ± 2.2) was skimmed before entering the interaction region where the dicarbon and silylidyne beams crossed perpendicularly giving a collision energy (E_c) of 42.9 ± 1.8 kJ mol^{-1} and center-of-mass (CM) angle (Θ_{CM}) of 47.8 ± 1.1°.

Our molecular beam contains both the $X^1\Sigma_g^+$ and $a^3\Pi_u$ states of dicarbon, which are only separated by 8 kJ mol^{-1}. While the ratio between singlet and triplet dicarbon within the beam is not known, the rovibrational distributions of the singlet and triplet states were measured previously using laser-induced fluorescence.[8,9] First, the singlet state was probed via the Mulliken excitation ($D^1\Sigma_u^+ - X^1\Sigma_g^+$). The fractions of v = 0 and v = 1 were 0.83 ± 0.10 and 0.17 ± 0.04, respectively, where the rotational distributions were bimodal in each case, giving rotational temperatures of 200 K (population fraction 0.44 ± 0.05) and 1000 K (population fraction 0.39 ± 0.05) for v = 0 and 200 K (population fraction 0.06 ± 0.02) and 1000 K (population fraction 0.11 ± 0.02) for v = 1. The triplet excited state of dicarbon was probed via the Swan band transition ($d^3\Pi_g - a^3\Pi_u$). The values reported for v = 0 and v = 1 were 240 K and 190 K with fractions of 0.67 ± 0.05 in v = 0 and 0.33 ± 0.05 in v = 1.

In addition to dicarbon, the primary reactant beam contains tricarbon molecules (C_3) and carbon atoms (C) produced during the laser ablation process. Furthermore, the secondary reactant beam may also contain silane (SiH_4) and silyl radicals (SiH_3) generated from the photolysis of

disilane.[10,11] Possible reactions of carbon with silylidyne, silyl, and silane would create products at lower m/z than detected for the title reaction (m/z = 52), and the reaction of carbon with disilane forms products (Si_2CH_4 / $SiCH_2$) which cannot fragment to m/z = 52. Thus, carbon reactions do not interfere with the target system. While tricarbon reactions with disilane, silane, silyl, and silylidyne may all contribute in principle to m/z = 52 signal from fragmentation of the parent products, only the case of the tricarbon reaction with silylidyne produced signal at m/z = 64 (SiC_3^+) under similar experimental conditions, i.e. reactions of tricarbon with disilane, silane, and silylidyne did not occur or their products did not fragment within the ionizer. This leaves fragmentation of products from the tricarbon–silylidyne reaction as the only possible contributor to m/z = 52 from reactions involving tricarbon. Lastly, dicarbon reactions with disilane, silane, silyl, and silylidyne may all contribute to observations at m/z = 52; however, no signal was observed at m/z = 53 or 54, rendering the dicarbon–silyl and dicarbon–silane[12] reactions insignificant for the experimental conditions.

A triply differentially pumped mass spectrometric detector—which is rotatable in the plane defined by both reactant beams—collected the reactively scattered products. Electron impact ionization at 80 eV and emission current of 2 mA ionized the products before mass filtering via a quadrupole mass spectrometer (150QC, Extrel) operating in the time-of-flight (TOF) mode and detection with a Daly-type particle ion counter.[13] Up to 4.4×10^6 TOF spectra were collected at each angle in 3–5° steps for the range $27° \leq \Theta \leq 65°$ with respect to the dicarbon beam ($\Theta = 0°$). Normalizing the TOF peak areas to the CM angle created a laboratory angular distribution (LAD). In order to obtain information on the chemical dynamics, the laboratory data were fit using a forward convolution routine, in which user-defined CM translational energy ($P(E_T)$) and angular ($T(\theta)$) flux distributions were refined iteratively until a reasonable fit of the data was achieved.[14,15] The image of the overall outcome of the reaction was developed from these functions, defined as $I(u,\theta) = P(u) \times T(\theta)$, and is portrayed as a flux contour map.[16]

Geometry optimizations were carried out with the ORCA[17] package employing the double-hybrid density functional B2PLYP[18], with the atom-pairwise dispersion correction with Becke-Johnson damping (D3BJ)[19,20]. The def2-TZVP[21] basis set was employed for these calculations. At this same level of theory, a vibrational analysis was performed to obtain the harmonic frequencies and zero-point energies (ZPE) for each structure. Additionally, intrinsic reaction coordinate (IRC) calculations were performed for the transition states to confirm their connections to the relevant

structures. To improve the accuracy of the relative energies, a single-point energy refinement was performed. This involved using the explicitly correlated coupled-cluster singles and doubles plus perturbative triples (CCSD(T)-F12)[22,23] method, along with the aug-cc-pV(Q+d)Z[24] basis set. This refinement was executed using the MOLPRO[25] software.

The C_2 + Si_2H_6 Reaction

The reaction of dicarbon (C_2, $X^1\sum_g^+$ / $a^3\Pi_u$) with disilane (Si_2H_6, X^1A_{1g}) was explored under similar conditions as the title reaction. Specifically, the dicarbon beam featured slightly different characteristics (1786 ± 18 m s^{-1} velocity (v_p) and 6.0 ± 0.4 speed ratio (S)), and the disilane beam was generated using pure disilane (99.998%, Air Liquide, v_p = 742 ± 35 m s^{-1}, S = 7.2 ± 0.7) at a backing pressure of 550 Torr. This resulted in a collision energy of 32.4 ± 1.0 kJ mol^{-1} and center-of-mass angle of 47.8 ± 1.6°. The reaction time-of-flight (TOF) spectra were collected at a mass-to-charge ratio (m/z) of 84 ($C_2Si_2H_4^+$). This detection can be attributed to the formation of $C_2Si_2H_4$ product(s) (84 amu) coupled with molecular hydrogen (2 amu) loss. TOFs were obtained in 5° steps from 23° to 63° with respect to the dicarbon beam and normalized to the center-of-mass angle, giving a laboratory angular distribution (LAD) (Figure S1). The TOFs are about 300 μs wide, while the LAD features a range of about 50°. This distribution is symmetric with respect to the center-of-mass angle indicating that the dicarbon plus disilane reaction is indirect, involving formation of $C_2Si_2H_6$ intermediate(s) before H_2 loss to $C_2Si_2H_4$ product(s).

Converting the laboratory data into the center-of-mass reference frame yields additional information on the reactive scattering dynamics. This process provides product translational energy ($P(E_T)$) and angular flux ($T(\theta)$) distributions (Figure S2). These functions are used to fit the laboratory data, which could be fit with a single reaction channel via molecular hydrogen loss. The $P(E_T)$ shows a maximum translational energy at 263 ± 46 kJ mol^{-1}, which results in a reaction energy of −231 ± 47 kJ mol^{-1} when considering the conservation of energy. The $P(E_T)$ also peaks at about 45 kJ mol^{-1}, indicating that products are formed through a tight exit transition state with substantial electron density rearrangement. The $T(\theta)$ reveals an indirect, isotropic scattering distribution, where equal probability of scattering at any angle indicates long-lived intermediate(s) with lifetime(s) greater than their rotational period(s).

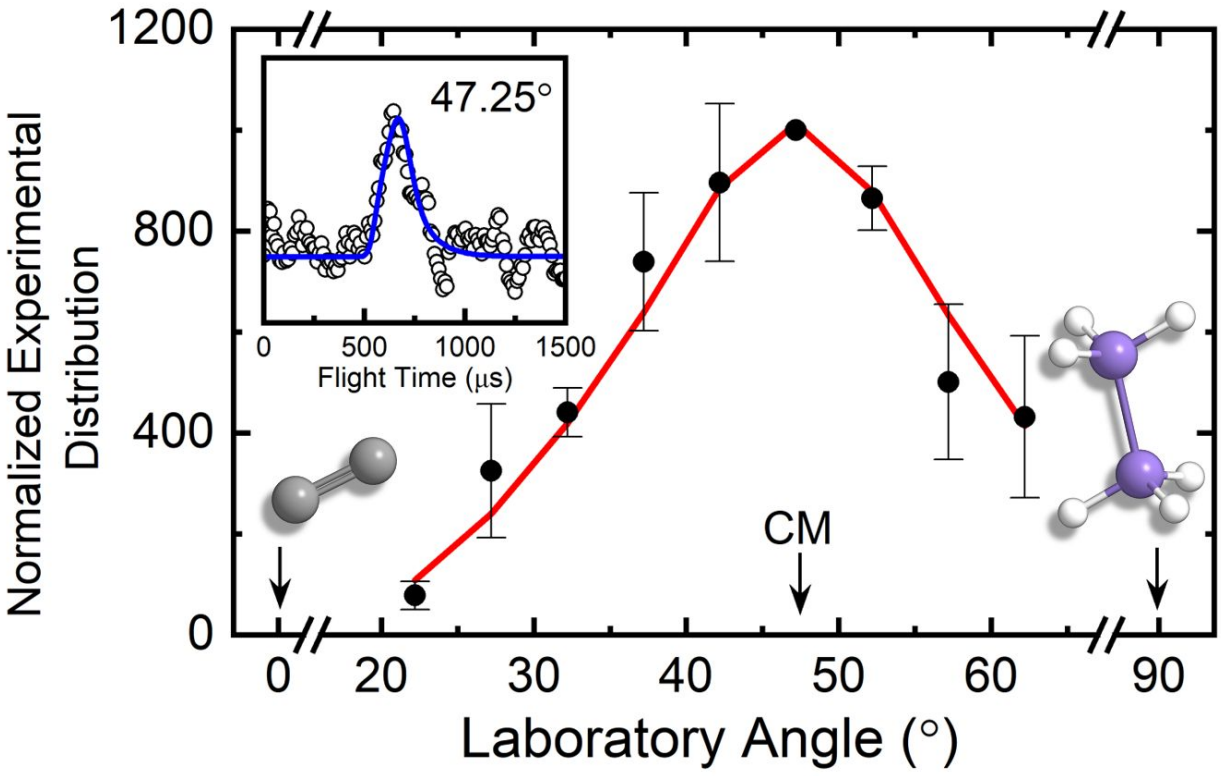

Figure S1. Laboratory angular distribution and time-of-flight (TOF) spectrum (inset) recorded at mass-to-charge (m/z) = 84 for the reaction of dicarbon (C_2) with disilane (Si_2H_6). CM represents the center-of-mass angle, and 0° and 90° define the directions of the dicarbon and disilane beams, respectively. The black circles depict the data and red and blue lines the experimental fits.

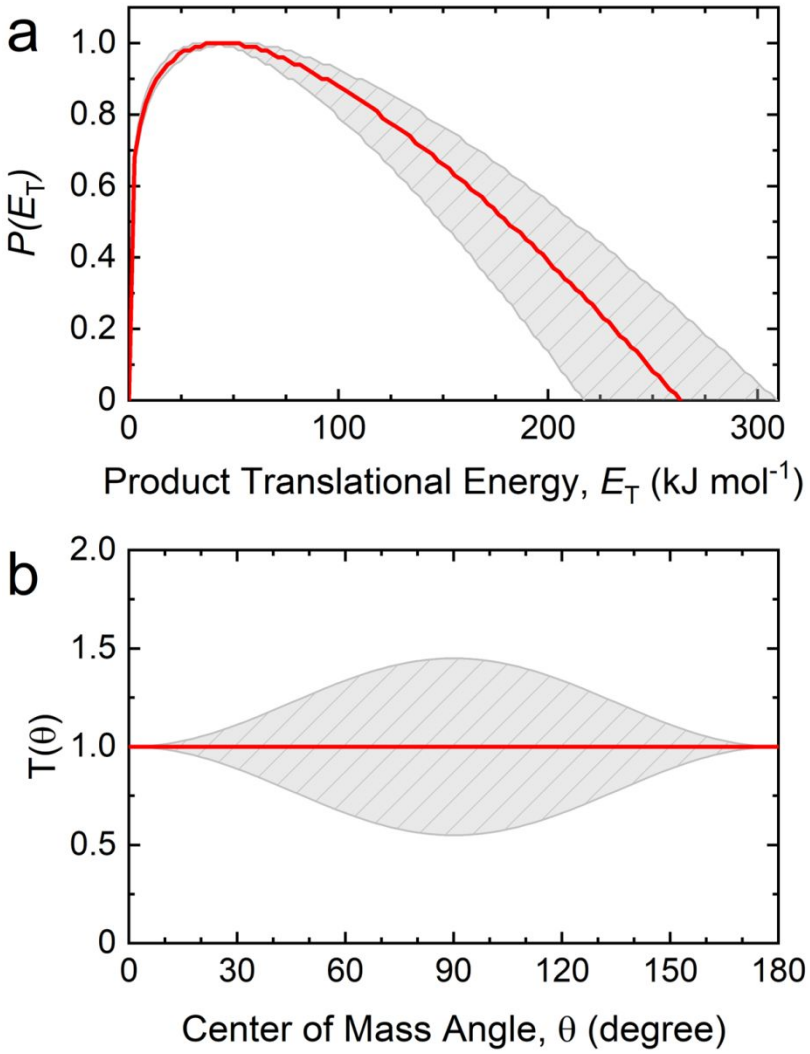

Figure S2. Center-of-mass product translational energy (**a**) and angular (**b**) flux distributions leading to the formation of $C_2Si_2H_4$ isomer(s) in the reaction of dicarbon (C_2) with disilane (Si_2H_6). Red lines define the best-fit functions while shaded areas provide the error limits.

Data S1. Optimized Cartesian coordinates (Å) and vibrational frequencies (cm^{-1}) of reactants, products, intermediates, and transition states involved in the dicarbon (C_2) plus silylidyne (SiH) reaction.

Reactants

C2($X^1\Sigma g+$)

C	-7.974996	1.185965	0.000000
C	-6.807544	1.647495	0.000000

1847.79 cm**-1

C2($a^3\Pi u$)

C	-8.000095	1.176043	0.000000
C	-6.782445	1.657417	0.000000

1661.65 cm**-1

SiH($X^2\Pi r$)

Si	-7.648134	2.139903	0.000000
H	-6.254456	2.753927	0.000000

2054.29 cm**-1

Products

---

p1 - C2Si(C2v, ^{1}A_1)

Si	-3.510449	2.612679	0.000000
C	-4.281316	0.939109	0.000000
C	-3.017185	0.837532	0.000000

Frequencies:

206.53 cm**-1

800.46 cm**-1

1791.47 cm**-1

p2 - C2H(C_inf_v, $^2\Sigma g+$)

C	-7.328191	0.982057	-0.000000
C	-6.128255	0.896746	0.000000
H	-5.067816	0.820373	-0.000000

Frequencies:

608.94 cm**-1

2109.07 cm**-1

3475.74 cm**-1

p3 - C2Si(C_inf_v, $^3\Pi$)

Si	-10.108963	1.031132	0.000000
C	-8.326477	0.780213	-0.000000

C -7.102751 0.610345 0.000000

Frequencies:

273.64 cm**-1

627.34 cm**-1

1956.94 cm**-1

Doublet minima

D1 - (Cs, ²A')

Si	0.000000	-0.032028	-1.023796
H	0.000000	1.228788	-1.827630
C	-0.000001	0.081940	0.671498
C	0.000001	-0.040761	1.944308

Frequencies:

109.74 cm**-1

157.49 cm**-1

691.29 cm**-1

780.17 cm**-1

1908.21 cm**-1

2135.44 cm**-1

D2 - (Cs, ²A')

Si	0.000265	-0.124263	-0.767392
H	-0.000169	0.914177	-1.848033
C	0.000104	0.723869	0.885179
C	-0.000200	-0.555264	1.014186

Frequencies:

178.46 cm**-1

267.64 cm**-1

735.37 cm**-1

771.86 cm**-1

1692.96 cm**-1

2108.32 cm**-1

D3 - (Cs, ²A')

Si	-0.000451	-1.163985	-0.981933
H	0.000599	1.471600	0.068465
C	-0.000306	-0.701023	0.812521
C	0.000159	0.393408	0.100948

Frequencies:

598.29 cm**-1

690.23 cm**-1

790.24 cm**-1

875.13 cm**-1

1583.23 cm**-1

3245.38 cm**-1

D4 - (C_inf_v, X²Π)

Si	0.116856	-0.684601	-1.383553
H	-0.191073	1.184413	2.248965
C	-0.020213	0.140363	0.219266
C	-0.111795	0.699094	1.305397

Frequencies:

229.87 cm**-1

569.84 cm**-1

620.94 cm**-1

776.49 cm**-1

1997.77 cm**-1

3457.40 cm**-1

Doublet TS

D1-D2

Si	-0.000713	-0.388092	-0.931072
H	0.001386	1.047952	-1.365649
C	-0.001495	-0.812676	0.727942
C	0.000823	0.152816	1.568778

Frequencies:

-137.51 cm**-1 ***imaginary mode***

106.28 cm**-1

669.80 cm**-1

925.50 cm**-1

1804.90 cm**-1

2102.25 cm**-1

D2-D3

Si	0.000066	-0.677393	-0.725060
H	-0.000024	0.810394	-1.213438
C	-0.000054	0.532010	0.733985
C	0.000012	-0.665011	1.204513

Frequencies:

-915.14 cm**-1 ***imaginary mode***

261.81 cm**-1

369.82 cm**-1

714.59 cm**-1

1666.84 cm**-1

1775.61 cm**-1

D3-D4

Si	0.000080	0.107954	-0.994719
C	-0.000005	-0.666420	0.736344
C	-0.000118	0.333380	1.468859
H	0.000043	1.143590	2.165396

Frequencies:

-412.47 cm**-1 ***imaginary mode***

678.32 cm**-1

756.71 cm**-1

779.45 cm**-1

1879.18 cm**-1

3410.68 cm**-1

Quartet minima

Q1 - (Cs, ^{4}A")

Si	-0.000002	-0.030396	-1.051146
H	-0.000001	1.219663	-1.841901
C	0.000008	0.115849	0.721368
C	-0.000005	-0.067177	1.936059

Frequencies:

225.05 cm**-1

285.82 cm**-1

669.10 cm**-1

681.37 cm**-1

2001.78 cm**-1

2218.69 cm**-1

Q2 - (Cs, ^{4}A")

Si	-0.503920	0.082578	-0.766499
H	0.332820	0.711436	-1.831621
C	-0.214090	0.656529	1.044898
C	0.385190	-0.492022	0.837162

Frequencies:

493.01 cm**-1

606.88 cm**-1

615.32 cm**-1

674.69 cm**-1

1560.46 cm**-1

2128.32 cm**-1

Q3 - (Cs, ^{4}A")

Si	-0.000462	-1.194409	-0.991055
H	0.000605	1.478292	0.102233
C	-0.000297	-0.683630	0.817354
C	0.000155	0.399746	0.071469

Frequencies:

539.29 cm**-1

633.79 cm**-1

641.62 cm**-1

815.12 cm**-1

1502.94 cm**-1

3245.27 cm**-1

Q4 - (C_inf_v $X^4\Sigma^-$)

Si	0.114362	-0.669870	-1.354827
H	-0.190048	1.177837	2.236285
C	-0.019779	0.138176	0.214922
C	-0.110761	0.693125	1.293696

Frequencies:

290.15 cm**-1

629.22 cm**-1

633.30 cm**-1

668.35 cm**-1

2080.93 cm**-1

3489.07 cm**-1

Quartet TS

Q1-Q2

Si	-0.359699	-0.237625	-0.753866
H	0.174644	0.705786	-1.771932
C	-0.041885	0.332327	1.013965
C	0.226939	-0.800488	1.511832

Frequencies:

-487.86 cm**-1 ***imaginary mode***

330.69 cm**-1

651.10 cm**-1

668.62 cm**-1

1796.76 cm**-1

2165.52 cm**-1

Q2-Q3

Si	-0.005444	-0.063353	-0.900449
H	1.042265	0.887968	-0.035492
C	-0.035371	0.671569	0.957202
C	0.017429	-0.629194	1.120715

Frequencies:

-778.15 cm**-1 ***imaginary mode***

260.05 cm**-1

418.11 cm**-1

780.81 cm**-1

1486.10 cm**-1

1538.64 cm**-1

Q3-Q4

Si	0.561874	-0.943778	-1.408822
H	0.272192	0.558389	1.467064
C	-0.729634	0.095289	-0.561749
C	-0.104433	0.290100	0.503507

Frequencies:

-425.93 cm**-1 ***imaginary mode***

594.36 cm**-1

676.40 cm**-1

795.91 cm**-1

1760.85 cm**-1

3402.42 cm**-1

Supporting References

(1) Gu, X.; Guo, Y.; Kaiser, R. I. Mass spectrum of the butadiynyl radical (C_4H; $X^2\sum^+$). *Int. J. Mass Spectrom.* **2005**, *246*, 29.

(2) Gu, X.; Kaiser, R. I. Reaction dynamics of phenyl radicals in extreme environments: A crossed molecular beam study. *Acc. Chem. Res.* **2009**, *42*, 290.

(3) Kaiser, R. I.; Stranges, D.; Bevsek, H. M.; Lee, Y. T.; Suits, A. G. Crossed-beam reaction of carbon atoms with hydrocarbon molecules. IV. Chemical dynamics of methylpropargyl radical formation, C_4H_5, from reaction of $C(^3P_j)$ with propylene, C_3H_6 (X^1A). *J. Chem. Phys.* **1997**, *106*, 4945.

(4) Kaiser, R. I.; Stranges, D.; Lee, Y. T.; Suits, A. G. Crossed-beam reaction of carbon atoms with hydrocarbon molecules. II. Chemical dynamics of n-C_4H_3 formation from reaction of $C(^3P_j)$ with methylacetylene, CH_3CCH (X^1A_1). *J. Chem. Phys.* **1996**, *105*, 8721.

(5) Huang, L. C. L.; Balucani, N.; Lee, Y. T.; Kaiser, R. I.; Osamura, Y. Crossed beam reaction of the cyano radical, $CN(X^2\Sigma^+)$, with methylacetylene, CH_3CCH (X^1A_1): Observation of cyanopropyne, CH_3CCCN (X^1A_1), and cyanoallene, $H_2CCCHCN$ (X^1A'). *J. Chem. Phys.* **1999**, *111*, 2857.

(6) Stahl, F.; Schleyer, P. v. R.; Bettinger, H. F.; Kaiser, R. I.; Lee, Y. T.; Schaefer III, H. F. Reaction of the ethynyl radical, C_2H, with methylacetylene, CH_3CCH, under single collision conditions: Implications for astrochemistry. *J. Chem. Phys.* **2001**, *114*, 3476.

(7) Kaiser, R. I.; Hahndorf, I.; Huang, L. C. L.; Lee, Y. T.; Bettinger, H. F.; Schleyer, P. v. R.; Schaefer, H. F., III; Schreiner, P. R. Crossed beams reaction of atomic carbon, $C(^3P_j)$, with d_6-benzene, $C_6D_6(X^1A_{1g})$: Observation of the per-deutero-1,2-didehydro-cycloheptatrienyl radical, $C_7D_5(X^2B_2)$. *J. Chem. Phys.* **1999**, *110*, 6091.

(8) Dangi, B. B.; Maity, S.; Kaiser, R. I.; Mebel, A. M. A combined crossed beam and ab initio investigation of the gas phase reaction of dicarbon molecules (C_2; $X^1\Sigma_g^+/a^3\Pi_u$) with propene (C_3H_6; X^1A'): identification of the resonantly stabilized free radicals 1-and 3-vinylpropargyl. *J. Phys. Chem. A* **2013**, *117*, 11783.

(9) Kaiser, R. I.; Maksyutenko, P.; Ennis, C.; Zhang, F.; Gu, X.; Krishtal, S. P.; Mebel, A. M.; Kostko, O.; Ahmed, M. Untangling the chemical evolution of Titan's atmosphere and surface–From homogeneous to heterogeneous chemistry. *Faraday Discuss.* **2010**, *147*, 429.

(10) Tada, N.; Tonokura, K.; Matsumoto, K.; Koshi, M.; Miyoshi, A.; Matsui, H. Photolysis of disilane at 193 nm. *J. Phys. Chem. A* **1999**, *103*, 322.

(11) Muranaka, Y.; Motooka, T.; Lubben, D.; Greene, J. E. Ultraviolet-laser photolysis of disilane. *J. Appl. Phys.* **1989**, *66*, 910.

(12) Rettig, A.; Head-Gordon, M.; Doddipatla, S.; Yang, Z.; Kaiser, R. I. Crossed beam experiments and computational studies of pathways to the preparation of singlet ethynylsilylene (HCCSiH; X^1A'): The silacarbene counterpart of triplet propargylene (HCCCH; X^3B). *J. Phys. Chem. Lett.* **2021**, *12*, 10768.

(13) Daly, N. R. Scintillation type mass spectrometer ion detector. *Rev. Sci. Instrum.* **1960**, *31*, 264.

(14) Vernon, M. F. Molecular beam scattering. Ph.D. Dissertation, University of California at Berkeley, Berkeley, CA, **1983**.

(15) Weiss, P. S. Reaction dynamics of electronically excited alkali atoms with simple molecules. Ph.D. Dissertation, University of California at Berkeley, Berkeley, CA, **1985**.

(16) Kaiser, R. I. Experimental investigation on the formation of carbon-bearing molecules in the interstellar medium via neutral−neutral reactions. *Chem. Rev.* **2002**, *102*, 1309.

(17) Neese, F. Software update: The ORCA program system—Version 5.0. *WIREs Comput. Mol. Sci.* **2022**, *12*, e1606.

(18) Grimme, S. Semiempirical hybrid density functional with perturbative second-order correlation. *J. Chem. Phys.* **2006**, *124*.

(19) Becke, A. D.; Johnson, E. R. A density-functional model of the dispersion interaction. *J. Chem. Phys.* **2005**, *123*.

(20) Grimme, S.; Ehrlich, S.; Goerigk, L. Effect of the damping function in dispersion corrected density functional theory. *J. Comput. Chem.* **2011**, *32*, 1456.

(21) Weigend, F.; Ahlrichs, R. Balanced basis sets of split valence, triple zeta valence and quadruple zeta valence quality for H to Rn: Design and assessment of accuracy. *Phys. Chem. Chem. Phys.* **2005**, *7*, 3297.

(22) Adler, T. B.; Knizia, G.; Werner, H.-J. A simple and efficient CCSD(T)-F12 approximation. *J. Chem. Phys.* **2007**, *127*, 221106.

(23) Knizia, G.; Adler, T. B.; Werner, H.-J. Simplified CCSD(T)-F12 methods: Theory and benchmarks. *J. Chem. Phys.* **2009**, *130*, 054104.

(24) Dunning Jr., T. H.; Peterson, K. A.; Wilson, A. K. Gaussian basis sets for use in correlated molecular calculations. X. The atoms aluminum through argon revisited. *J. Chem. Phys.* **2001**, *114*, 9244.

(25) Werner, H. J.; Knowles, P. J.; Knizia, G.; Manby, F. R.; Schütz, M.; Celani, P.; Györffy, W.; Kats, D.; Korona, T.; Lindh, R.; Mitrushenkov, A.; Rauhut, G.; Shamasundar, K. R.; Adler, T. B.; Amos, R. D.; Bernhardsson, A.; Berning, A.; Cooper, D. L.; Deegan, J. O.; Dobbyn, A. J.; Eckert, F.; Goll, E.; Hampel, C.; Hesselmann, A.; Hetzer, G.; Hrenar, T.; Jansen, G.; Köppl, C.; Liu, Y.; Lloyd, A. W.; Mata, R. A.; May, A. J.; McNicholas, S. J.; Meyer, W.; Mura, M. E.; Nicklass, A.; O'Neill, D. P.; Palmieri, P.; Peng, D.; Pflüger, K.; Pitzer, R.; Reiher, M.; Shiozaki, T.; Stoll, H.; Stone, A. J.; Tarroni, R.; Thorsteinsson, T.; Wang, M. *MOLPRO, a package of ab initio programs*, Version 2015.1; University of Cardiff: Cardiff, UK, **2015**; see http://www.molpro.net.